Large-Scale Synthesis and Microwave Absorption Enhancement of Actinomorphic Tubular ZnO/$CoFe_2O_4$ Nanocomposites

Jing Cao, Wuyou Fu,* Haibin Yang, Qingjiang Yu, Yanyan Zhang, Shikai Liu, Peng Sun, Xiaoming Zhou, Yan Leng, Shuangming Wang, Bingbing Liu, and Guangtian Zou

State Key Laboratory of Superhard Materials, Jilin University, Changchun 130012, PR China

Received: October 22, 2008; Revised Manuscript Received: January 14, 2009

Actinomorphic tubular ZnO/$CoFe_2O_4$ nanocomposites were fabricated in large scale via a simple solution method at low temperature. The phase structures, morphologies, particle size, shell thickness, chemical compositions of the composites have been characterized by X-ray diffraction (XRD), field emission scanning electron microscope (FESEM), energy dispersive X-ray spectroscopy (EDS), and transmission electron microscopy (TEM). The as-synthesized nanocomposites were uniformly dispersed into the phenolic resin then the mixture was pasted on metal plate with the area of 200 mm × 200 mm as the microwave absorption test plate. The test of microwave absorption was carried out by the radar-absorbing materials (RAM) reflectivity far field radar cross-section (RCS) method. The range of microwave absorption is from 2 to 18 Hz and the best microwave absorption reach to 28.2 dB at 8.5 Hz. The results indicate that the composites are of excellence with respect to microwave absorption.

Introduction

Along with the development of scientific technology and modern society, the problem of electromagnetic interference has became more and more serious due to wide applications of electromagnetic waves in the GHz range for mobile phone, local area network, radar systems, and also television image interference of high-rise buildings, microwave dark-room, and so on.[1−3] Therefore, microwave absorbing materials are not only applied to the stealth technology of military[4] but also used in the people's production and life in all aspects. On the basis of these reasons, the demands to develop more economical electromagnetic wave absorbers with wider absorbing bandwidths and more effective absorbing are ever increasing. In the past years, extensive study has been carried out to develop new microwave absorbing materials with a high magnetic and electric loss.[5−9] Soft magnet $CoFe_2O_4$ ferrite has a large saturation magnetization and high Snoek's limit, which results in high complex permeability values at a wide frequency range. This factor makes $CoFe_2O_4$ highly useful as a thin absorber working at a high-frequency band.[10,11] However, magnet $CoFe_2O_4$ ferrite is quite heavy, which restricts their usefulness in the applications requiring lightweight mass.[12] In recent years, it has been shown that magnetic nanocomposites are used as microwave absorbing materials due to their advantages in respect to lightweight, low cost, design flexibility, and microwave absorption properties over pure ferrites.[12] It is well-known, some research work has been focused on one-dimensional (1D) nanostructure ZnO, which can be used as microwave absorbing materials.[13] The large scale synthesis of ZnO is easily realized and the cost of preparation process for commercial application is very low. So ZnO is promising and vivid as a microwave absorption material. Many different morphological 1D ZnO nanomaterials have been fabricated by using various approaches.[14−24] Compared with other structures, tubular structures exhibit higher porosity, thus provide an effective way to optimize the performances of electromagnetic wave absorbing materials. On the basis of these characteristics, novel electromagnetic wave absorption properties are expected from ZnO nanotubes/$CoFe_2O_4$ nanocomposites. However, to date, large scale preparation of ZnO nanotubes/$CoFe_2O_4$ nanocomposites is still overlooked in literature, and the related properties investigations are still absent.

In the present work, we report for the first time the actinomorphic tubular ZnO/$CoFe_2O_4$ nanocomposites by a simple chemical solution method. Characterization was accomplished using various techniques, such as powder X-ray diffraction, scanning electron microscopy, X-ray energy-dispersive spectroscopy, and so on. Moreover, the aim of this paper is to develop the core−shell structure materials based on ZnO and $CoFe_2O_4$ using the two-step coprecipitation method and investigate their magnetic properties and microwave absorption characteristics.

Experimental Section

Materials. Zinc nitrate and hexamethylenetetramine (HMT) were purchased from Beijing Chemicals Co. Ltd. Cobalt nitrate ($Co(NO_3)_2 \cdot 4H_2O$), iron nitrate ($Fe(NO_3)_3 \cdot 9H_2O$), sodium hydroxide (NaOH) of analytical reagent grade were obtained from Beijing Chemical Corporation. All reagents were used without further purification. Distilled water was used in all the experiments.

Preparation of Actinomorphic Tubular ZnO/$CoFe_2O_4$ Nanocomposites. Synthesis of the ZnO nanotubes was based on our previous study,[25] in which 100 mL of aqueous solution of zinc nitrate and 100 mL of hexamethylenetetramine (HMT) aqueous solution of equal concentration (0.1 M) were mixed together and kept under mild magnetic stirring for 5 min. Then, the solution was transferred into a 500 mL flask and heated at 90 °C for 24 h with refluxing. Subsequently, the resulting white products were centrifuged, washed with deionized water and ethanol two times and dried at 60 °C in air for further characterization. Whereafter, a simple chemical solution reaction was employed to build actinomorphic tubular ZnO/$CoFe_2O_4$

* To whom correspondence should be addressed. E-mail address: fuwy@jlu.edu.cn. Tel.: +86 431 85168763. Fax: +86 431 85168763.

10.1021/jp8093287 CCC: $40.75
Published on Web 03/16/2009

nanocomposite bundles with a coprecipitation method. First, 100 mL of iron nitrate aqueous solution (0.005 M) and 100 mL of cobalt nitrate aqueous solution (0.0025 M) were mixed together and kept under mild mechanical stirring for 5 min. Then the fabricated ZnO nanotubes bundles of 0.9 g were immersed in the prepared solution at room temperature for 1 h concomitant stirring. This mixture was slowly added to 100 mL of 0.08 M NaOH solution, and this mixture was transferred into a 500 mL flask and kept at 90 °C for 2 h, sealed, with nonstop stirring. The mixture was allowed to cool to room temperature. Subsequently the resulting products were washed and centrifuged with deionized water and ethanol two times and dried at 80 °C in air for further characterization.

Preparation of Microwave Test Plate. Pure $CoFe_2O_4$, actinomorphic tubular ZnO/$CoFe_2O_4$ nanocomposites, whose ZnO mass fraction were 40, 60, and 80 wt %, and pure ZnO were uniformly dispersed into the ethanol solution of phenolic resin, respectively. Then the mixture was painted on a metal plate with the area of 200 mm × 200 mm, and the spreading thickness was 1.5 mm. To make the microwave test plate, the mixture was solidified for 24 h at 80 °C to obtain microwave test plate nos. 1, 2, 3, 4, and 5, respectively.

Characterization. The products were characterized by X-ray diffraction (XRD), which was conducted on a Rigaku D/max-2500 X-ray diffractometer with Cu Kα radiation ($\lambda = 1.5418$ Å). Field-emission scanning electron microscopy (FESEM), it was obtained on a JEOL JEM-6700F microscope operating at 5 KV. X-ray energy-dispersive spectroscopy (EDX) attached to SEM, while EDS analysis was performed to understand their chemical constituents. Transmission electron microscopy (TEM) was obtained on a JEOL JEM-2000EX microscope. The magnetization measurements were carried out at room temperature by using a vibrating sample magnetometer (model TM-VSM1230-HHHS) with a maximum applied field of 15 kOe. Reflection loss was measured using a HP8510C network vector analyzer working at the 2∼18 GHz band. The remaining sample was pressed full circle for complex relative permittivity ($\varepsilon_r = \varepsilon' - j\varepsilon''$) and permeability ($\mu_r = \mu' - j\mu''$) measurements, with the American HP8722 microwave network vector analyzer determination of the sample complex magnetic permeability and the duplicate coefficient of dielectrical loss; the sweep frequency scope is 2∼18 GHz, each 0.5 GHz surveys data.

Result and Discussion

XRD Patterns. The X-ray powder diffraction patterns of the as-prepared pure ZnO, $CoFe_2O_4$, and actinomorphic tubular ZnO/$CoFe_2O_4$ nanocomposites are shown in Figure 1a−g, respectively. In Figure 1a, the diffraction peaks at 31.8°, 34.45°, and 36.35° come from ZnO (JCPDS 79-0205). No diffraction peaks from other crystalline forms are detected, which indicates a high purity and crystallinity of these ZnO samples. In Figure 1b, the diffraction peaks at 30.25°, 35.55°, 43.40°, 57.15°, and 62.75° come from $CoFe_2O_4$ nanoparticles (JCPDS 22-1086), all diffraction peaks can be indexed to a typical spinel structured $CoFe_2O_4$. In Figure 1c, the diffraction peaks corresponding to both ZnO and $CoFe_2O_4$ can be seen clearly. From Figure 1c, we can obtain that, although the two diffraction peaks position of $CoFe_2O_4$ at $2\theta = 35.55°$ (main peak) and ZnO at $2\theta = 36.35°$ (main peak) are quite close to each other, the existence of the two peaks can be still seen clearly. Besides, there are no other diffraction peaks except ZnO and $CoFe_2O_4$. Figure 1 panels d−g show the ZnO/$CoFe_2O_4$ composites in which the content of ZnO is 20, 40, 60, and 80 wt %, respectively. It is can be seen that when the content of ZnO is 40 and 60 wt %, the peaks of ZnO and $CoFe_2O_4$ can be seen clearly. When the content of ZnO is 80 wt %, the peaks belonging to $CoFe_2O_4$ are not obvious due to the low relative content of $CoFe_2O_4$, but we can distinguish the existence of the peaks at 35.55° and 43.40° belonging to $CoFe_2O_4$ at curve of ZnO 80 wt %. Likewise, when the content of ZnO is 20 wt %, the peaks belonging to ZnO are not obvious due to the low relative content of ZnO, but we can distinguish the existence of the peaks at 31.8° and 47.65°, which belong to ZnO at the curve of ZnO 20 wt%. In addition, the peaks at 35.55°, 57.15°, and 62.75° broaden significantly, because ZnO and $CoFe_2O_4$ both have peaks close to each other around these places. Hence, it is concluded that the as-synthesized core/shell structured composites are composed of crystalline ZnO and $CoFe_2O_4$.

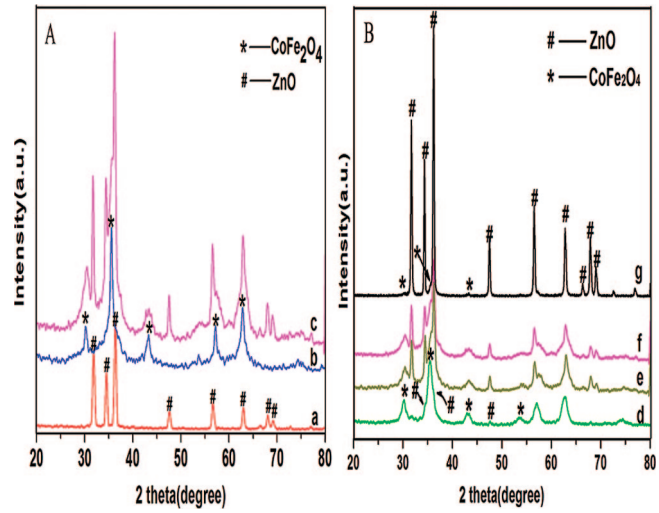

Figure 1. XRD patterns of (a) pure ZnO nanotube bundles, (b) pure $CoFe_2O_4$ nanoparticles, (c) actinomorphic tubular ZnO/$CoFe_2O_4$ nanocomposites, and (d−g) ZnO/$CoFe_2O_4$ composites in which the content of ZnO is 20, 40, 60, and 80 wt %, respectively.

Morphologies, Particle Size, and Chemical Compositions Analysis. The magnified FESEM images shown in Figure 2a and 2c indicate the detailed morphology of pure ZnO and the ZnO/$CoFe_2O_4$ nanotube bundles. As can be seen from Figure 2a, the wall thickness of the ZnO nanotubes is about 60 nm, inner diameters of the tubes are about 350 nm, and each tube outer wall has the obvious six edge angles, which because of ZnO have a hexagonal structure.[25] In comparison with Figure 2a, the average length of the ZnO nanotubes has not obviously changed (Figure 2c), while the six edge angles of the outer wall have disappeared, and some small particles can clearly be found on the surface of the ZnO nanotube. It indicates that ZnO nanotubes have been coated with $CoFe_2O_4$ nanoparticles, and the size of $CoFe_2O_4$ nanoparticles are below 40 nm (inset a of Figure 2c). EDX patterns of a single nanotube for these two samples are also shown in Figure 2b and 2d to get the composition of the samples. The EDX pattern of the ZnO nanotubes shows only the presence of O and Zn elements. Co and Fe elements are found to be present after the nanotube is coated with $CoFe_2O_4$ nanoparticles, which provides powerful evidence for the successful coating of $CoFe_2O_4$ on the surface of ZnO nanotubes. This is consistent with the broad peaks of $CoFe_2O_4$ in the XRD spectra (Figure 1b,c). It can be seen that the coating of $CoFe_2O_4$ nanoparticles is continuous and uniform. Figure 3 shows the magnified FESEM images of ZnO/$CoFe_2O_4$ composites with different relative content of ZnO. It can be seen that with the decreasing of relative content of ZnO, the coating thickness increases significantly. However, in compari-

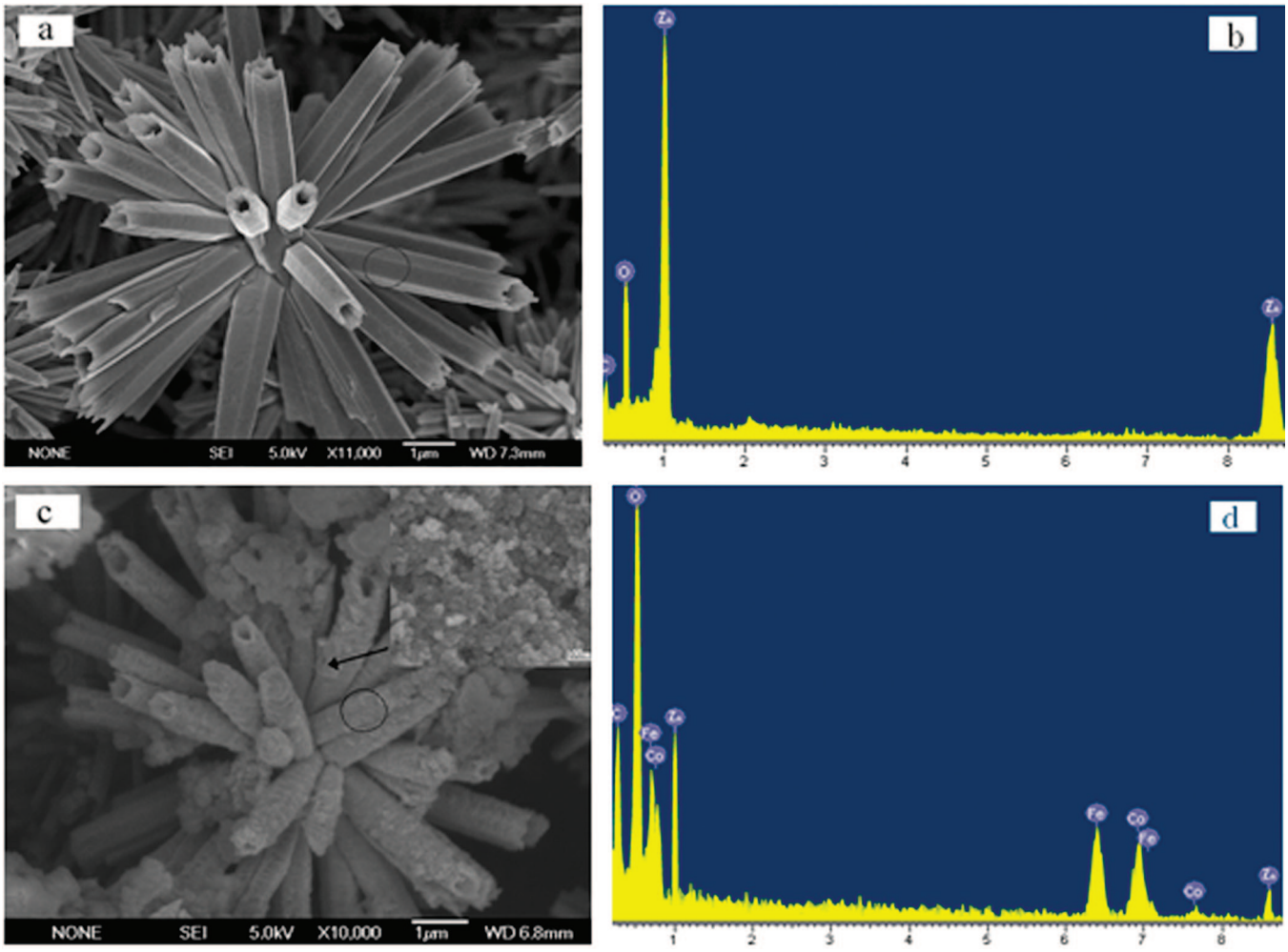

Figure 2. (a,c) Magnified FESEM images of ZnO nanotubes and ZnO nanotubes/$CoFe_2O_4$ (insets show the circled areas magnified several times); (b,d) EDX of ZnO nanotubes and ZnO nanotubes/$CoFe_2O_4$, respectively.

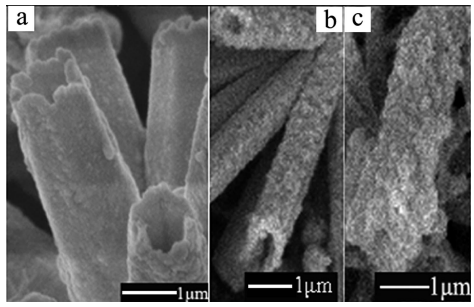

Figure 3. Magnified FESEM images of ZnO/$CoFe_2O_4$ composites with different relative content of ZnO: (a) 80%; (b) 60%; (c) 40%.

son with Figure 2a, the tubular structures are not obviously changed. Figure 4 is a TEM image of typical area of actinomorphic tubular ZnO/$CoFe_2O_4$ nanocomposites. It can be seen that $CoFe_2O_4$ is coating the surface of ZnO (average 100 nm thick) as a thin layer. It also illustrates that $CoFe_2O_4$ nanoparticles coat ZnO nanotubes compactly, and there is no obvious crack in the core−shell of the ZnO/$CoFe_2O_4$ structure. This is in agreement with the result which is concluded from SEM.

Magnetic Property. The magnetic properties of the as-synthesized $CoFe_2O_4$ and the representative actinomorphic tubular ZnO/$CoFe_2O_4$ nanocomposites were measured at room temperature as shown in Figure 5. In the case of $CoFe_2O_4$ nanoparticles, saturated magnetization ($\mathbf{M}_s$), remnant magnetization ($\mathbf{M}_r$) and coercive force ($\mathbf{H}_c$) were estimated to be $\mathbf{M}_s$ =

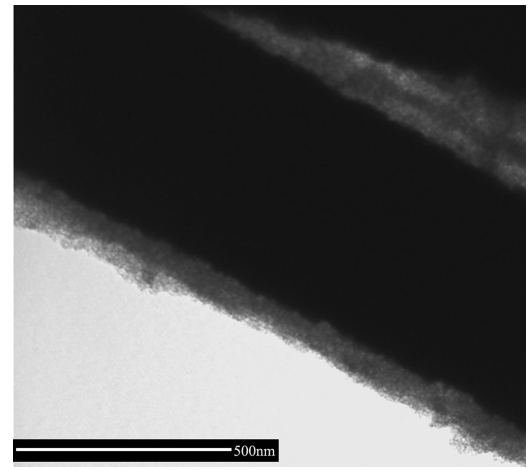

Figure 4. TEM image of the typical area of the actinomorphic tubular ZnO/$CoFe_2O_4$ nanocomposites.

63.0 emu/g, $\mathbf{M}_r$ = 10.0 emu/g and $\mathbf{H}_c$ = 193.0 emu/g, respectively. A similar behavior for the actinomorphic tubular ZnO/$CoFe_2O_4$ nanocomposites was observed. In contrast, $\mathbf{M}_s$ of the ZnO coated with $CoFe_2O_4$ decreased to 27 emu/g, mainly due to the volume of the nonmagnetic to the total sample volume.

Microwave Absorption Property. Figure 6 is the RAM reflectivity far field RCS method spectrum of five microwave test plates. Number 1 test plate is the pure $CoFe_2O_4$ nanoparticles

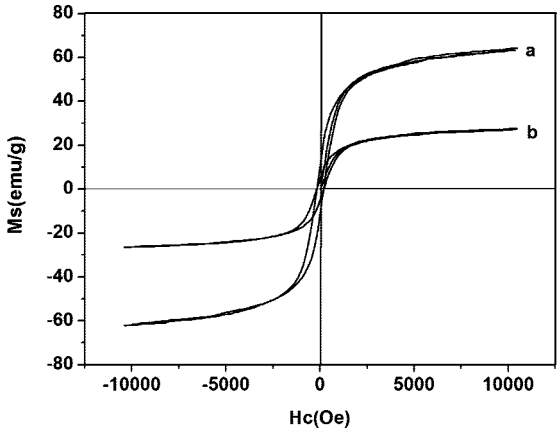

Figure 5. Magnetization curves of (a) pure $CoFe_2O_4$; (b) actinomorphic tubular ZnO/$CoFe_2O_4$ nanocomposites.

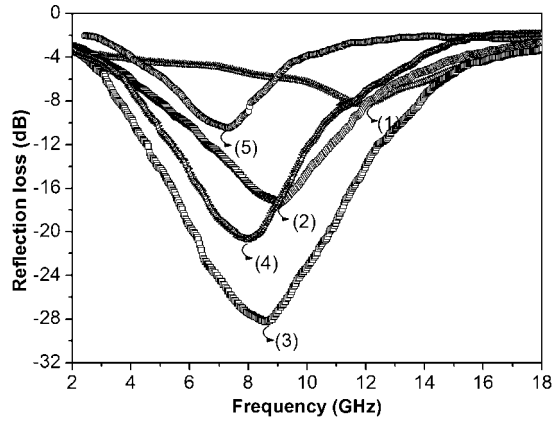

Figure 6. Reflection loss determined in the phenolic cement: (1) pure $CoFe_2O_4$ nanoparticles; actinomorphic tubular ZnO/$CoFe_2O_4$ nanocomposites in which content of ZnO is (2) 40 wt %, (3) 60 wt %, (4) 80 wt%; (5) pure ZnO nanotubes bundles.

as the microwave absorbents. Numbers 2, 3, and 4 test plates are ZnO/$CoFe_2O_4$ composites in which the content of ZnO is 40, 60, and 80 wt % as the microwave absorbents and will be designated as ZC1, ZC2, and ZC3, separately. Number 5 test plate is pure ZnO nanotubes bundles as the microwave absorbents. It can be seen that the reflection loss of pure ZnO nanotubes and $CoFe_2O_4$ nanoparticles are rather low for all frequencies between 2∼18 GHz and the peak values are 8.3 and 10.5 dB, respectively. For actinomorphic tubular ZnO/$CoFe_2O_4$ nanocomposites, the microwave absorption is evidently improved (much better than that of both ZnO nanotubes and $CoFe_2O_4$ particles). As shown in Figure 6, the sample ZC1 shows the maximum reflection loss of 17.2 dB at 9.1 GHz, the sample ZC2 shows the maximum reflection loss of 28.3 dB at 8.6 GHz, and the sample ZC3 shows the maximum reflection loss of 20.6 dB at 8.0 GHz. The maximum reflection loss increases from 10.5 dB to about 28.3 dB for the weight ratio of $CoFe_2O_4 \leq 40\%$. When the weight ratio of ZnO is 60%, the composites have good compatible dielectric and magnetic properties, and hence the microwave absorbing properties show the maximum value. However, when the weight ratio of ZnO is 40%, the maximum reflection loss decreases to 17.2 dB, which may be due to deteriorating the dielectric property when the weight ratio of $CoFe_2O_4$ exceeds a critical value. Hence, the $CoFe_2O_4$ particle-functionalized ZnO nanotubes exhibit a better microwave absorption. The improvement of microwave absorption obviously originates from the combination of ZnO nanotubes and $CoFe_2O_4$ nanoparticles. Therefore, the difference on reflection loss maximum as a function of the samples is associated with the magnetocrystalline anisotropy and structure anisotropy of as-synthesized ZnO nanotubes/$CoFe_2O_4$ nanocomposites. Compared with that of pure ZnO nanotubes and $CoFe_2O_4$ nanoparticles, enhanced microwave absorption of actinomorphic tubular ZnO/$CoFe_2O_4$ nanocomposites at 2∼18 GHz was observed and the possible mechanism was discussed.

Complex Relative Permittivity and Permeability. To investigate the possible mechanisms and effects about the enhancement of microwave absorption, we independently measured the complex relative permittivity and permeability of the samples. Figure 7 shows the real and imaginary parts of permittivity (ε', ε'') and permeability (μ', μ'') spectra of pure $CoFe_2O_4$-phenolic cement composites and ZnO/$CoFe_2O_4$ (weight ratio of ZnO = 40%, 60%, 80%, 100%)-phenolic cement composites. As shown in Figure 7, the real parts of the permittivity of the specimens remain almost constant in the whole frequency range, where the ε' largely increases with the increase of the weight ratio of ZnO. Compared with the pure $CoFe_2O_4$, ZnO has high ε'. So the existence of ZnO will result in the large increase of ε'. Compared with the pure $CoFe_2O_4$, the imaginary parts of the complex relative permittivity for ZnO/$CoFe_2O_4$ (weight ratio of ZnO = 40%, 60%, 80%, 100%)-phenolic cement composites show a small resonance peak at 9.1, 8.4, 7.9, and 7.1 GHz, for samples 2, 3, 4, 5, respectively. We analyzed the mechanism of the change in the ε' and ε'' with frequency for ZnO/$CoFe_2O_4$ (weight ratio of ZnO = 0% 40%, 60%, 80%, 100%)-wax composites. First, it has been shown in the previous paper[26,27] that the properties of interfaces could have a dominant role in determining dielectric performance. The characteristic feature of the ZnO is dielectric materials; the dominant dipolar polarization and the associated relaxation phenomena constitute the loss mechanisms. Composite materials, in which dielectric nanotubes coated with magnetic particles nanolayers, additional dielectric interfaces, and more polarization charges on the surface of the particles make the behaviors of dielectric relaxation more complex. Second, since the ZnO nanotubes/$CoFe_2O_4$ nanocomposites is a heterogeneous system, interfacial polarization is an important polarization process and associated relaxation also will give rise to loss mechanism. The real and imaginary parts of the complex permeability are shown in Figure 7c,d. Either the real part or the imaginary parts of the complex relative permeability of the ZnO/$CoFe_2O_4$ composites is lower than that of pure $CoFe_2O_4$. The lower values of the complex relative permeability for the ZnO/$CoFe_2O_4$ composites observed in these samples may be attributed to the presence of nonmagnetic polymer between the neighboring crystallites which weakens the intergranular magnetic interaction. We can find that μ'' largely increases with the increase of the weight ratio of $CoFe_2O_4$ in the whole frequency range. This result can be explained by the magnetic dissipation. According to Vander Zaag's suggestion,[28] the magnetic dissipation of ferrite includes hysteresis loss, eddy current loss, residual loss, ferromagnetic resonance loss, and domain wall loss.In this study, however, the enhancement of conductance of ZnO nanotubes/$CoFe_2O_4$ nanocomposites might contribute to higher μ'' of the ZnO nanotubes/CoFe2O4 nanocomposites-phenolic cement composites because of ZnO nanotubes/CoFe2O4 being a magnetic semiconductor. The normalized input impedance Z_{in} of a metal-backed microwave absorption layer could be obtained from the following expression: $Z_{in} = (\mu_r/\varepsilon_r)^{1/2} \tanh[j(2\pi/c)(\mu/\varepsilon_r)^{1/2}fd]$ where μ_r and ε_r are the

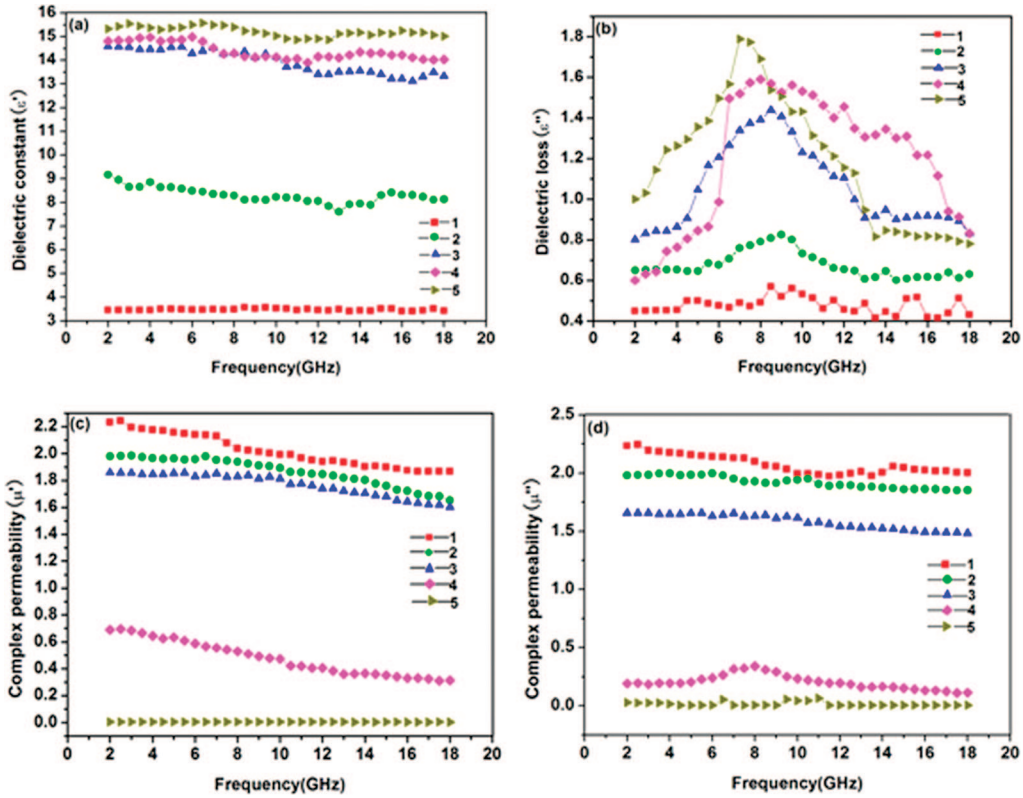

Figure 7. (a) Real (ε') and (b) imaginary (ε'') parts of the relative complex permittivity, (c) real (μ') and (d) imaginary (μ'') parts of the relative complex permeability of ZnO/$CoFe_2O_4$ composites in which the weight ratio of ZnO is 0% (1), 40% (2), 60% (3), 80% (4), and 100% (5).

relative permeability and permittivity of the composite medium, c is the velocity of electromagnetic waves in free space, f is the frequency of microwaves, and d is the thickness of the absorber. Accordingly, the reflection loss is associated with Z_{in} as *reflection loss* $(dB) = 20 \log Z_{in} - 1/Z_{in} + 1$.[29,30] It can be seen that the microwave absorption would be improved when the magnetic contribution matches the dielectric contribution based on the requirement of the tanh mathematics function, that is, $\tanh[j(2\pi/c)(\mu/\varepsilon_r)^{1/2}fd]$. With the combined effect of dielectric dissipation ZnO nanotubes and magnetic dissipation of $CoFe_2O_4$ nanoparticles, when the weight ratio of $CoFe_2O_4$ is 40%, the microwave absorbency of the ZnO nanotubes/$CoFe_2O_4$ nanocomposites−phenolic cement composites shows the maximum value.

Conclusion

In summary, large-scale actinomorphic tubular ZnO/$CoFe_2O_4$ nanocomposites were successfully prepared, in which core ZnO nanotubes bundles were synthesized by a single solution method at a mild temperature of 90 °C, and shell $CoFe_2O_4$ nanoparticles were produced at low temperature without using any catalysts, templates, or substrates. The microwave absorption properties of pure $CoFe_2O_4$, actinomorphic tubular ZnO/$CoFe_2O_4$ nanocomposites in which ZnO mass fraction were 40, 60, and 80 wt % and pure ZnO were investigated, and the results indicate that the composites are excellent with respect to microwave absorption. Taking actinomorphic tubular ZnO/$CoFe_2O_4$ nanocomposites as the microwave absorbent, the microwave absorption is higher than 28 GHz. Compared with pure $CoFe_2O_4$, it can not only greatly reduce the mass of microwave absorbing materials, but also enhance the microwave absorption effect. The $CoFe_2O_4$-coated ZnO nanotube bundles have promise in their potential application to lightweight and strong absorption microwave absorbers.

Acknowledgment. The authors are grateful for the financial support from the Doctoral Foundation New Teacher project (200801831006) and National Basic Research Program of China (2005 CB724400).

References and Notes

(1) Liu, Z. F.; Bai, G.; Huang, Y.; Li, F. F.; Ma, Y. F.; Guo, T. Y.; He, X. B.; Lin, X.; Gao, H. J.; Chen, Y. S. *J. Phys. Chem. C* **2007**, *111*, 13696–13700.
(2) Motojima, S.; Hoshiya, S.; Hishikawab, Y. *Carbon* **2003**, *41*, 2653–2689.
(3) Xu, P.; Han, X.; Jiang, J.; Wang, X.; Li, X.; Wen, A. *J. Phys. Chem. C* **2007**, *111*, 12603–12608.
(4) Wen, H.; Cao, M. H.; Sun, G. B.; Xu, W. G.; Wang, D.; Zhang, X. Q.; Hu, C. W. *J. Phys. Chem. C* **2008**, *112*, 15948–15955.
(5) Purcell, W. P.; Fish, K.; Smyth, C. P. *J. Am. Chem. Soc.* **1960**, *82*, 6299–6301.
(6) Heston, W. M., Jr.; Smyth, C. P. *J. Am. Chem. Soc.* **1950**, *72*, 99–101.
(7) Grubb, E. L.; Smyth, C. P. *J. Am. Chem. Soc.* **1961**, *83* (20), 4122–4124.
(8) Kalman, O. F.; Smyth, C. P. *J. Am. Chem. Soc.* **1960**, *82* (4), 783–787.
(9) Roberti, D. M.; Smyth, C. P. *J. Am. Chem. Soc.* **1960**, *82* (9), 2106–2110.
(10) Wan, J.; Wang, X.; Wu, Y.; Zeng, M.; Wang, Y.; Jiang, H.; Zhou, W.; Wang, G.; Liu, J. *Appl. Phys. Lett.* **2005**, *86*, 122501.
(11) Manova, E.; Kunev, B.; Paneva, D.; Mitov, I.; Petrov, L. *Chem. Mater.* **2004**, *16*, 5689.
(12) Fu, W. Y.; Liu, S. K.; Fan, W. H.; Yang, H. B.; Pang, X. F.; Xu, J.; Zou, G. T. *J. Magn. Magn. Mater.* **2007**, *316*, 54.
(13) Zhuo, R. F.; Feng, H. T.; Chen, J. T.; Yan, D.; Feng, J. J.; Li, H. J.; Geng, B. S.; Cheng, S.; Xu, X. Y.; Yan, P. X. *J. Phys. Chem. C* **2008**, *112* (31), 11767–11775.
(14) Zhang, H.; Yang, D.; Ma, X.; Du, N.; Wu, J.; Que, D. *J. Phys. Chem. B* **2006**, *110* (2), 827–830.
(15) Zhang, Y.; Jia, H.; Luo, X.; Chen, X.; Yu, D.; Wang, R. *J. Phys. Chem. B* **2003**, *107* (33), 8289–8293.
(16) Zhang, H.; Yang, D.; Ji, Y.; Ma, X.; Xu, J.; Que, D. *J. Phys. Chem. B* **2004**, *108* (13), 3955–3958.
(17) Gao, P.; Wang, Z. L. *J. Phys. Chem. B* **2002**, *106* (49), 12653–12658.

(18) Jiang, C.; Zhang, W.; Zou, G.; Yu, W.; Qian, Y. *J. Phys. Chem. B* **2005**, *109* (4), 1361–1363.

(19) Zhang, Y.; Wang, L.; Liu, X.; Yan, Y.; Chen, C.; Zhu, J. *J. Phys. Chem. B* **2005**, *109* (27), 13091–13093.

(20) Han, X. H.; Wang, G. Z.; Jie, J. S.; Luo, Y.; Yuk, T. I.; Choy, W. C. H.; Hou, J. G. *J. Phys. Chem. B* **2005**, *109* (7), 2733–2738.

(21) Sun, X. H.; Lam, S.; Sham, T. K.; Heigl, F.; Jurgensen, A.; Wong, N. B. *J. Phys. Chem. B* **2005**, *109* (8), 3120–3125.

(22) Huang, H.; Yang, S.; Gong, J.; Liu, H.; Duan, J.; Zhao, X.; Zhang, R.; Liu, Y.; Liu, Y. *J. Phys. Chem. B* **2005**, *109* (44), 20746–20750.

(23) Jie, J. S.; Wang, G. Z.; Han, X. H.; Hou, J. G. *J. Phys. Chem. B* **2004**, *108* (44), 17027–17031.

(24) Song, J. H.; Wang, X. D.; Riedo, E.; Wang, Z. L. *J. Phys. Chem. B* **2005**, *109* (20), 9869–9872.

(25) Yu, Q. J.; Fu, W. Y.; Yu, C. L.; Yang, H. B.; Wei, R. H.; Li, M. H.; Liu, S. K.; Sui, Y. M.; Liu, Z. L.; Yuan, M. X.; Zou, G. T. *J. Phys. Chem. C* **2007**, *111*, 17521–17526.

(26) Lewis, T. J. *J. Phys. D: Appl. Phys.* **2005**, *38*, 202.

(27) Kim, S.; Yoon, Y. J. *J. Appl. Phys.* **2005**, *97*, 10F905.

(28) Vander Zaag, PJ. J. *Magn. Magn. Mater.* **1999**, *315*, 196–197.

(29) Miles, P. A.; Westphal, W. B.; Hippel, A. V. *Rev. Mod. Phys.* **1957**, *29*, 279.

(30) Ishino, K.; Narumiya, Y. *Ceram. Bul.* **1987**, *66*, 1469.

JP8093287